Semiclassical Boltzmann transport theory for multi-Weyl semimetals

Sanghyun Park, Seungchan Woo, E. J. Mele, and Hongki Min

Semiclassical Boltzmann transport theory for multi-Weyl semimetals

Sanghyun Park[1], Seungchan Woo[1], E. J. Mele[2], and Hongki Min[1,2*]

[1] *Department of Physics and Astronomy, Seoul National University, Seoul 08826, Korea and*

[2] *Department of Physics and Astronomy, University of Pennsylvania, Philadelphia, PA 19104, USA*

(Dated: April 5, 2017)

Multi-Weyl semimetals (m-WSMs) are a new type of Weyl semimetal that have linear dispersion along one symmetry direction but anisotropic non-linear dispersion along the two transverse directions with a topological charge larger than one. Using the Boltzmann transport theory and fully incorporating the anisotropy of the system, we study the DC conductivity as a function of carrier density and temperature. We find that the characteristic density and temperature dependence of the transport coefficients at the level of Boltzmann theory are controlled by the topological charge of the multi-Weyl point and distinguish m-WSMs from their linear Weyl counterparts.

Introduction — There has been a growing interest in three-dimensional (3D) analogs of graphene called Weyl semimetals (WSMs) where bands disperse linearly in all directions in momentum space around a twofold point degeneracy. Most attention has been devoted to novel response functions in elementary WSMs which exhibit a linear dispersion; however, recently it has been realized that these are just the simplest members of a family of multi-Weyl semimetals (m-WSMs)[1–3] which are characterized instead by double (triple) Weyl-nodes with a linear dispersion along one symmetry direction but quadratic (cubic) dispersion along the remaining two directions. These multi-Weyl nodes have a topologically protected charge (also referred to as chirality) larger than one, a situation that can be stabilized by point group symmetries[2].

Noting that multilayer graphenes with certain stacking patterns support 2D gapless low energy spectra with high chiralities, these m-WSMs can be regarded as the 3D version of multilayer graphenes. One can expect that their modified energy dispersion and spin- or pseudospin-momentum locking textures will have important consequences for various physical properties due both to an enhanced density of states (DOS) and the anisotropy in the energy dispersion, distinguishing m-WSMs from elementary WSMs. In this Rapid Communication, we demonstrate that this emerges already at the level of DC conductivity in the strong scattering limit described by semiclassical Boltzmann transport theory. The transport properties of conventional linear WSMs have recently been explored theoretically by several authors[4–13], and there have been theoretical works on the stability of charge-neutral double-Weyl nodes in the presence of Gaussian disorder[14–16] and the thermoelectric transport properties in double-Weyl semimetals[17]. However, as we show below, the density- and temperature-dependences of the DC conductivity for m-WSMs require an understanding of the effect of anisotropy in the nonlinear dispersion on the scattering. We develop this theory and find that it predicts characteristic power-law dependences of the conductivity on density and temperature that depend on the topological charge of the Weyl node and distinguish m-WSMs from their linear counterparts.

Model — The low-energy effective Hamiltonian for m-WSMs with chirality J near a single Weyl point is given by[1,2,18]

$$H_J = \varepsilon_0 \left[\left(\frac{k_-}{k_0} \right)^J \sigma_+ + \left(\frac{k_+}{k_0} \right)^J \sigma_- \right] + \hbar v_z k_z \sigma_z, \quad (1)$$

where $k_\pm = k_x \pm i k_y$, $\sigma_\pm = \frac{1}{2}(\sigma_x \pm i\sigma_y)$, $\boldsymbol{\sigma}$ are the Pauli matrices acting in the space of the two bands that make contact at the Weyl point, and k_0 and ε_0 are the material-dependent parameters in units of momentum and energy, respectively. For simplicity, here we assumed an axial symmetry around the k_z-axis. The eigenenergies of the Hamiltonian are given by $\varepsilon_\pm = \pm\varepsilon_0\sqrt{\tilde{k}_\parallel^{2J} + c_z^2\tilde{k}_z^2}$ where $\tilde{\boldsymbol{k}} = \boldsymbol{k}/k_0$, $\tilde{k}_\parallel = \sqrt{\tilde{k}_x^2 + \tilde{k}_y^2}$ and $c_z = \hbar v_z k_0/\varepsilon_0$, thus the Hamiltonian H_J has a linear dispersion along the k_z direction for $k_x = k_y = 0$, whereas a non-linear dispersion $\sim k_\parallel^J$ along the in-plane direction for $k_z = 0$. Note that the system described by the Hamiltonian in Eq. (1) has a non-trivial topological charge characterized by the chirality index J^2. [See Sec. I in Supplemental Material (SM)[19] for the eigenstates and DOS for m-WSMs.]

Boltzmann transport theory in anisotropic systems — We use semiclassical Boltzmann transport theory to calculate the density and temperature dependence of the DC conductivity, which is fundamental in understanding transport properties of a system. Here we focus on the longitudinal part of the DC conductivity assuming time-reversal symmetry with vanishing Hall conductivities. The Boltzmann transport theory is known to be valid in the high carrier density limit, and we assume that the Fermi energy is away from the Weyl node, as in most Weyl semimetals[20,21]. The limitation of the current approach will be discussed later.

For a d-dimensional *isotropic* system in which only a single band is involved in the scattering, it is well known that the momentum relaxation time at a wavevector $\boldsymbol{k}$ in the relaxation time approximation can be expressed[22]

$$\frac{1}{\tau_{\boldsymbol{k}}} = \int \frac{d^d k'}{(2\pi)^d} W_{\boldsymbol{k}\boldsymbol{k}'} (1 - \cos\theta_{\boldsymbol{k}\boldsymbol{k}'}), \quad (2)$$

where $W_{\boldsymbol{k}\boldsymbol{k}'} = \frac{2\pi}{\hbar} n_{\text{imp}} |V_{\boldsymbol{k}\boldsymbol{k}'}|^2 \delta(\varepsilon_{\boldsymbol{k}} - \varepsilon_{\boldsymbol{k}'})$, n_{imp} is the impurity density, and $V_{\boldsymbol{k}\boldsymbol{k}'}$ is the impurity potential describing

a scattering from $\boldsymbol{k}$ to $\boldsymbol{k'}$. The inverse relaxation time is a weighted average of the collision probability in which the forward scattering ($\theta_{\boldsymbol{kk'}} = 0$) receives reduced weight.

For an *anisotropic* system, the relaxation time approximation Eq. (2) does not correctly describe the effects of the anisotropy on transport. Instead, coupled integral equations relating the relaxation times at different angles needs to be solved to treat the anisotropy in the non-equilibrium distribution[23,24]. The linearized Boltzmann transport equation for the distribution function $f_{\boldsymbol{k}} = f^{(0)}(\varepsilon) + \delta f_{\boldsymbol{k}}$ at energy $\varepsilon = \varepsilon_{\boldsymbol{k}}$ balances acceleration on the Fermi surface against the scattering rates

$$(-e)\boldsymbol{E}\cdot\boldsymbol{v}_{\boldsymbol{k}}S^{(0)}(\varepsilon) = \int \frac{d^d k'}{(2\pi)^d} W_{\boldsymbol{kk'}}\left(\delta f_{\boldsymbol{k}} - \delta f_{\boldsymbol{k'}}\right), \quad (3)$$

where $S^{(0)}(\varepsilon) = -\frac{\partial f^{(0)}(\varepsilon)}{\partial \varepsilon}$, $f^{(0)}(\varepsilon) = \left[e^{\beta(\varepsilon-\mu)} + 1\right]^{-1}$ is the Fermi distribution function at equilibrium, and $\beta = \frac{1}{k_{\mathrm{B}}T}$. We parameterize $\delta f_{\boldsymbol{k}}$ in the form:

$$\delta f_{\boldsymbol{k}} = (-e)\left(\sum_{i=1}^{d} E^{(i)} v_{\boldsymbol{k}}^{(i)} \tau_{\boldsymbol{k}}^{(i)}\right) S^{(0)}(\varepsilon), \quad (4)$$

where $E^{(i)}$, $v_{\boldsymbol{k}}^{(i)}$, and $\tau_{\boldsymbol{k}}^{(i)}$ are the electric field, velocity, and relaxation time along the i-th direction, respectively. After matching each coefficient in $E^{(i)}$, we obtain an integral equation for the relaxation time:

$$1 = \int \frac{d^d k'}{(2\pi)^d} W_{\boldsymbol{kk'}}\left(\tau_{\boldsymbol{k}}^{(i)} - \frac{v_{\boldsymbol{k'}}^{(i)}}{v_{\boldsymbol{k}}^{(i)}}\tau_{\boldsymbol{k'}}^{(i)}\right). \quad (5)$$

For the isotropic case [$\tau_{\boldsymbol{k}}^{(i)} = \tau(\varepsilon)$ for a given energy $\varepsilon = \varepsilon_{\boldsymbol{k}}$], Eq. (5) reduces to Eq. (2). [See Sec. II in SM[19] for applications of Eq. (5) to m-WSMs.] The current density $\boldsymbol{J}$ induced by an electric field $\boldsymbol{E}$ is then given by

$$J^{(i)} = g \int \frac{d^d k}{(2\pi)^d}(-e)v_{\boldsymbol{k}}^{(i)}\delta f_{\boldsymbol{k}} \equiv \sigma_{ij}E^{(j)}, \quad (6)$$

where g is the degeneracy factor and σ_{ij} is the conductivity tensor given by

$$\sigma_{ij} = ge^2 \int \frac{d^d k}{(2\pi)^d} S^{(0)}(\varepsilon) v_{\boldsymbol{k}}^{(i)} v_{\boldsymbol{k}}^{(j)} \tau_{\boldsymbol{k}}^{(j)}. \quad (7)$$

For the calculation, we set $g = 4$ and $v_z = v_0 \equiv \frac{\varepsilon_0}{\hbar k_0}$.

Density dependence of DC conductivity — Consider the m-WSMs described by Eq. (1) with chirality J and their DC conductivity as a function of carrier density at zero temperature. Due to the anisotropic energy dispersion with the axial symmetry, for $J > 1$ the conductivity also will be anisotropic as $\sigma_{xx} = \sigma_{yy} \neq \sigma_{zz}$.

We consider two types of impurity scattering: short-range impurities (e.g., lattice defects, vacancies, and dislocations) and charged impurities distributed randomly in the background. The impurity potential for short-range scatterers is given by a constant $V_{\boldsymbol{kk'}} = V_{\mathrm{short}}$ in

momentum space (i.e. zero-range delta-function in real space), whereas for charged Coulomb impurities in 3D it is given by $V_{\boldsymbol{kk'}} = \frac{4\pi e^2}{\epsilon(\boldsymbol{q})|\boldsymbol{q}|^2}$, where $\epsilon(\boldsymbol{q})$ is the dielectric function for $\boldsymbol{q} = \boldsymbol{k} - \boldsymbol{k'}$. Within the Thomas-Fermi approximation, the dielectric function can be approximated as $\epsilon(\boldsymbol{q}) \approx \kappa\left[1 + (q_{\mathrm{TF}}^2/|\boldsymbol{q}|^2)\right]$, where κ is the background dielectric constant, $q_{\mathrm{TF}} = \sqrt{\frac{4\pi e^2}{\kappa}D(\varepsilon_{\mathrm{F}})}$ is the Thomas-Fermi wavevector, and $D(\varepsilon_{\mathrm{F}})$ is the DOS at the Fermi energy ε_{F}. The interaction strength for charged impurities can be characterized by an effective fine structure constant $\alpha = \frac{e^2}{\kappa\hbar v_0}$. Note that $q_{\mathrm{TF}} \propto \sqrt{g\alpha}$.
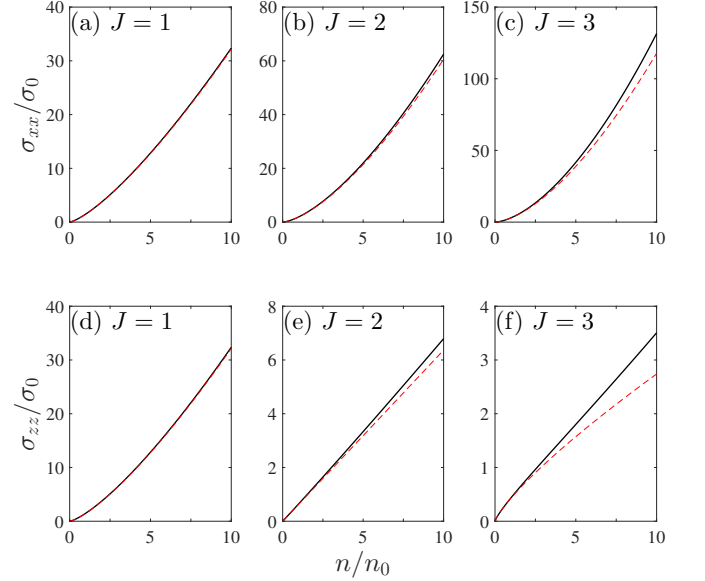
FIG. 1: Density dependence of DC conductivity (a)-(c) σ_{xx} and (d)-(f) σ_{zz} for charged impurities with $g\alpha = 1000$. Here, σ_0 and n_0 are density independent normalization constants in units of conductivity and density, respectively, defined in SM[19]. Red dashed lines represent analytic forms in the strong screening limit given by Eq. (24) in SM[19].

Figure 1 shows the density dependence of the DC conductivity for charged impurity scattering at zero temperature. Because of the chirality J, m-WSMs have a characteristic density dependence in DC conductivity, which can be understood as follows. From Eq. (7), we expect $\sigma_{ii} \sim [v_{\mathrm{F}}^{(i)}]^2/V_{\mathrm{F}}^2$ where $v_{\mathrm{F}}^{(i)}$ is the Fermi velocity along the i-th direction and V_{F}^2 is the angle-averaged squared impurity potential at the Fermi energy ε_{F}. For m-WSMs, the in-plane component with $k_z = 0$ and out-of-plane component with $k_x = k_y = 0$ for the velocity at ε_{F} are given by $v_{\mathrm{F}}^{(\|)} = Jv_0 r_{\mathrm{F}}^{1-\frac{1}{J}}$ and $v_{\mathrm{F}}^{(z)} = v_0 c_z$, respectively, where $r_{\mathrm{F}} = \varepsilon_{\mathrm{F}}/\varepsilon_0$. (See Sec. I in SM[19].)

For charged impurities, in the strong screening limit ($g\alpha \gg 1$), $V_{\mathrm{F}} \sim q_{\mathrm{TF}}^{-2} \sim D^{-1}(\varepsilon_{\mathrm{F}}) \sim \varepsilon_{\mathrm{F}}^{-\frac{2}{J}}$, thus we find

$$\sigma_{xx} \sim \varepsilon_{\mathrm{F}}^{2\left(1-\frac{1}{J}\right)}\varepsilon_{\mathrm{F}}^{\frac{4}{J}} \sim n^{\frac{2(J+1)}{J+2}}, \quad (8a)$$

$$\sigma_{zz} \sim \varepsilon_{\mathrm{F}}^{\frac{4}{J}} \sim n^{\frac{4}{J+2}}. \quad (8b)$$

Here, the DOS is $D(\varepsilon) \sim \varepsilon^{\frac{2}{J}}$, thus $\varepsilon_{\mathrm{F}} \sim n^{\frac{J}{J+2}}$. In the weak screening limit ($g\alpha \ll 1$), we expect $V_{\mathrm{F}} \sim \varepsilon_{\mathrm{F}}^{-2\zeta}$ with $\frac{1}{J} \leq \zeta \leq 1$, because the in-plane and out-of-plane components of the wavevector at ε_{F} are $k_{\mathrm{F}}^{(\parallel)} = k_0 r_{\mathrm{F}}^{\frac{1}{J}}$ and $k_{\mathrm{F}}^{(z)} = k_0 r_{\mathrm{F}}/c_z$, respectively. Thus, we find

$$\sigma_{xx} \sim \varepsilon_{\mathrm{F}}^{2\left(1-\frac{1}{J}\right)} \varepsilon_{\mathrm{F}}^{4\zeta} \sim n^{\frac{2(J-1)+4J\zeta}{J+2}}, \qquad (9a)$$

$$\sigma_{zz} \sim \varepsilon_{\mathrm{F}}^{4\zeta} \sim n^{\frac{4J\zeta}{J+2}}. \qquad (9b)$$

(See Sec. II in SM[19] for the analytic expressions of the DC conductivity for short-range impurities and for charged impurities in the strong screening limit, and detailed discussion for charged impurities in the weak screening limit.)
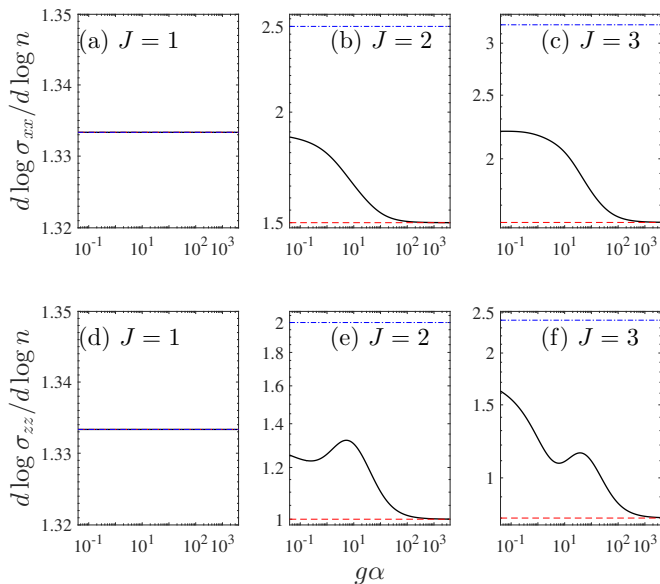
FIG. 2: (a)-(c) $d \log \sigma_{xx}/d \log n$ and (d)-(f) $d \log \sigma_{zz}/d \log n$ as a function of the screening strength $g\alpha$ for charged impurities. Red dashed and blue dash-dotted lines represent the density exponents obtained from $\zeta = \frac{1}{J}$ (or in the strong screening limit) and $\zeta = 1$ in Eq. (9), respectively. Here, $n = n_0$ is used for the calculation.

Figure 2 illustrates the evolution of the power-law density dependence of the DC conductivity as a function of the screening strength characterized by $g\alpha$. Note that $\zeta = \frac{1}{J}$ in Eq. (9) gives the same density exponent as in the strong screening limit in Eq. (8). Thus, as α increases, the density exponent evolves from that obtained in Eq. (9) with decreasing ζ within the range $\frac{1}{J} \leq \zeta \leq 1$. Here, non-monotonic behavior in the density exponent originates from the angle-dependent power-law in the relaxation time, which manifests in the weak screening limit. (See Sec. II in SM[19] for further discussion.)

Similarly, for short-ranged impurities, V_{F} is a constant independent of density; in this case we find

$$\sigma_{xx} \sim \varepsilon_{\mathrm{F}}^{2\left(1-\frac{1}{J}\right)} \sim n^{\frac{2(J-1)}{J+2}}, \qquad (10a)$$

$$\sigma_{zz} \sim \varepsilon_{\mathrm{F}}^{0} \sim n^{0}. \qquad (10b)$$
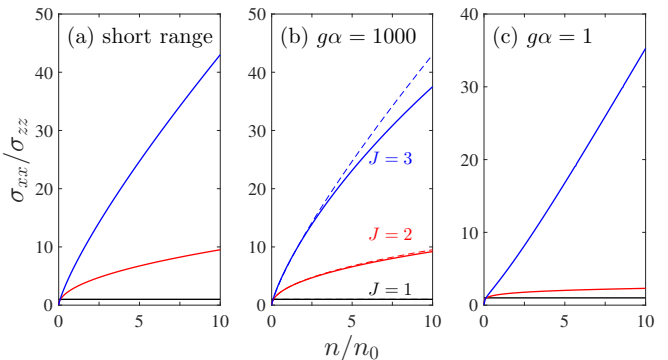
FIG. 3: σ_{xx}/σ_{zz} as a function of density for m-WSMs with $J = 1, 2, 3$ for (a) short-range impurities, (b) charged impurities with $g\alpha = 1000$, and (c) charged impurities with $g\alpha = 1$. Dashed lines in (b) represent analytic forms in the strong screening limit given by Eq. (24) in SM[19].

The anisotropy in conductivity can be characterized by σ_{xx}/σ_{zz}. Figure 3 shows σ_{xx}/σ_{zz} as a function of density for m-WSMs. Thus, as the carrier density increases, the anisotropy in conductivity increases. Interestingly, σ_{xx}/σ_{zz} for both short-range impurities and charged impurities in the strong screening limit is given by

$$\sigma_{xx}/\sigma_{zz} \sim \varepsilon_{\mathrm{F}}^{2\left(1-\frac{1}{J}\right)} \sim n^{\frac{2(J-1)}{J+2}}. \qquad (11)$$

Note that for arbitrary screening, ζs for σ_{xx} and σ_{zz} in Eq. (9) are actually different, thus not cancelled in σ_{xx}/σ_{zz} and the power-law deviates from that in Eq. (11). (See Sec. II in SM[19] for the analytic/asymptotic expressions of the density dependence of σ_{xx}/σ_{zz}.)

We consider both the short-range and charged impurities by adding their scattering rates according to Matthiessen's rule assuming that each scattering mechanism is independent. At low densities (but high enough to validate the Boltzmann theory) the charged impurity scattering always dominates the short-range scattering, while at high densities the short-range scattering dominates, irrespective of the chirality J and screening strength.

Temperature dependence of DC conductivity — In 3D materials, it is not easy to change the density of charge carriers by gating, because of screening in the bulk. However, the temperature dependence of DC conductivity can be used to understand carrier dynamics of the system. The effect of finite temperature arises from the energy averaging over the Fermi distribution function in Eq. (7), and the temperature dependence of the screening of the impurity potential for charged impurities[25,26].

From the invariance of carrier density with respect to temperature, we obtain the variation of the chemical potential $\mu(T)$ as a function of temperature T. Then the Thomas-Fermi wavevector $q_{\mathrm{TF}}(T)$ in 3D at finite T can be expressed $q_{\mathrm{TF}}(T) = \sqrt{\frac{4\pi e^2}{\kappa}\frac{\partial n}{\partial \mu}}$. In the low and high

temperature limits, the chemical potential is given by

$$\frac{\mu}{\varepsilon_{\mathrm{F}}} = \begin{cases} 1 - \frac{\pi^2}{3J}\left(\frac{T}{T_{\mathrm{F}}}\right)^2 & (T \ll T_{\mathrm{F}}), \\ \frac{1}{2\eta\left(\frac{2}{J}\right)\Gamma\left(2+\frac{2}{J}\right)}\left(\frac{T}{T_{\mathrm{F}}}\right)^{-\frac{2}{J}} & (T \gg T_{\mathrm{F}}), \end{cases} \quad (12)$$

whereas the Thomas-Fermi wavevector is given by

$$\frac{q_{\mathrm{TF}}(T)}{q_{\mathrm{TF}}(0)} = \begin{cases} 1 - \frac{\pi^2}{6J}\left(\frac{T}{T_{\mathrm{F}}}\right)^2 & (T \ll T_{\mathrm{F}}), \\ \sqrt{2\eta\left(\frac{2}{J}\right)\Gamma\left(1+\frac{2}{J}\right)}\left(\frac{T}{T_{\mathrm{F}}}\right)^{\frac{1}{J}} & (T \gg T_{\mathrm{F}}), \end{cases} \quad (13)$$

where $T_{\mathrm{F}} = \varepsilon_{\mathrm{F}}/k_{\mathrm{B}}$ is the Fermi temperature, and Γ and η are the gamma function and the Dirichlet eta function[27], respectively. (See Sec. III in SM[19] for the temperature dependence of the chemical potential and Thomas-Fermi wavevector.) In a single band system $q_{\mathrm{TF}}(T)$ always decreases with T^{-1} at high temperatures, whereas in m-WSMs $q_{\mathrm{TF}}(T)$ increases with $T^{\frac{1}{J}}$ because of thermal excitation of carriers that participate in the screening.
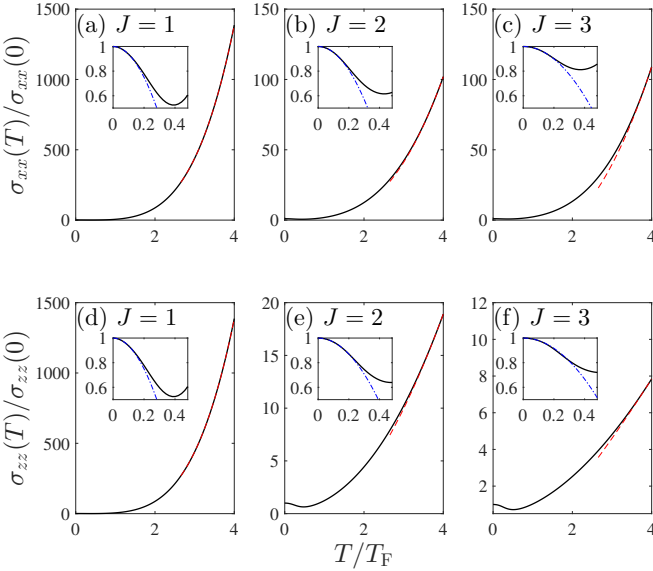
FIG. 4: Temperature dependence of DC conductivity (a)-(c) σ_{xx} and (d)-(f) σ_{zz} for charged impurities with $g\alpha = 1000$. Insets in each panel show the low temperature behavior. Red dashed and blue dash-dotted lines represent fitting by Eq. (14) with $\zeta = \frac{1}{J}$ in the high and low temperature limits, respectively.

Figure 4 shows the temperature dependence of DC conductivity for charged impurities. We find

$$\frac{\sigma_{xx}(T)}{\sigma_{xx}(0)} = \begin{cases} 1 + C_{xx}\left(\frac{T}{T_{\mathrm{F}}}\right)^2 & (T \ll T_{\mathrm{F}}), \\ D_{xx}\left(\frac{T}{T_{\mathrm{F}}}\right)^{2+4\zeta-\frac{2}{J}} & (T \gg T_{\mathrm{F}}), \end{cases} \quad (14a)$$

$$\frac{\sigma_{zz}(T)}{\sigma_{zz}(0)} = \begin{cases} 1 + C_{zz}\left(\frac{T}{T_{\mathrm{F}}}\right)^2 & (T \ll T_{\mathrm{F}}), \\ D_{zz}\left(\frac{T}{T_{\mathrm{F}}}\right)^{4\zeta} & (T \gg T_{\mathrm{F}}). \end{cases} \quad (14b)$$

As discussed, ζ varies within $\frac{1}{J} \leq \zeta \leq 1$ and approach $\frac{1}{J}$ in the strong screening limit ($g\alpha \gg 1$). Here, the high-temperature coefficients $D_{ii} > 0$, whereas the low-temperature coefficients C_{ii} change sign from negative to positive as α increases. For short-range impurities, we find

$$\frac{\sigma_{xx}(T)}{\sigma_{xx}(0)} = \begin{cases} 1 + C_{xx}^{\mathrm{short}}\left(\frac{T}{T_{\mathrm{F}}}\right)^2 & (T \ll T_{\mathrm{F}}), \\ D_{xx}^{\mathrm{short}}\left(\frac{T}{T_{\mathrm{F}}}\right)^{\frac{2(J-1)}{J}} & (T \gg T_{\mathrm{F}}), \end{cases} \quad (15a)$$

$$\frac{\sigma_{zz}(T)}{\sigma_{zz}(0)} = \begin{cases} 1 - e^{-T_{\mathrm{F}}/T} & (T \ll T_{\mathrm{F}}), \\ \frac{1}{2} + D_{zz}^{\mathrm{short}}\left(\frac{T}{T_{\mathrm{F}}}\right)^{-\frac{2+J}{J}} & (T \gg T_{\mathrm{F}}). \end{cases} \quad (15b)$$

Here, $C_{xx}^{\mathrm{short}} < 0$ and $D_{ii}^{\mathrm{short}} > 0$. Note that for $J = 1$, Eq. (15a) becomes constant, and reduces to Eq. (15b) if next order corrections are included. (See Sec. IV in SM[19] for the analytic/asymptotic expressions of the temperature coefficients, and the evolution of C_{ii} as a function of $g\alpha$.)

To understand the temperature dependence, we can consider a situation where the thermally induced charge carriers participate in transport. Then the temperature dependence in the high temperature limit can be obtained simply by replacing the ε_{F} dependence with T in Eqs. (8)-(10), which describe the density dependence of DC conductivity. Similarly as in Fig. 3, $\sigma_{xx}(T)/\sigma_{zz}(T)$ also increases with T at high temperatures.

For the charged impurities at high temperatures, and neglecting the effect of phonons, the conductivity increases with temperature, and mimics an insulating behavior. By contrast, for short-range impurities at high temperatures, $\sigma_{zz}(T)$ decreases with temperature and approaches $0.5\sigma_{zz}(0)$, thus showing a metallic behavior. Interestingly, $\sigma_{xx}(T)$ shows contrasting behavior for $J > 1$ and $J = 1$, increasing (decreasing) with temperature for $J > 1$ ($J = 1$) showing insulating (metallic) behavior at high temperatures.

Discussion — We find that the DC conductivities in the Boltzmann limit show characteristic density and temperature dependences that depend strongly on the chirality of the system, revealing a signature of m-WSMs in transport measurements, which can be compared with experiments. In real materials with time reversal symmetry, multiple Weyl points with compensating chiralities will be present. The contributions from the individual nodes calculated by our method are additive when the Weyl points are well separated and internode scattering is weak. Our analysis is based on the semiclassical Boltzmann transport theory with the Thomas-Fermi approximation for screening and corrected for the anisotropy of the Fermi surface in m-WSMs. The Boltzmann transport theory is known to be valid in the high density limit. At low densities, inhomogeneous impurities induce a spatially varying local chemical potential, typically giving a minimum conductivity when the chemical potential is at the Weyl node[12] and the problem is treated within the effective medium theory. Note that

the Thomas-Fermi approximation used in this work is the long-wavelength limit of the random phase approximation (RPA), and neglects interband contributions to the polarization function[12], thus deviating from the RPA result at low densities. Both simplifications become important in the low-density limit, which will be considered in our future work.

[*] Electronic address: hmin@snu.ac.kr

[1] G. Xu, H. Weng, Z. Wang, X. Dai, and Z. Fang, Chern Semimetal and the Quantized Anomalous Hall Effect in $HgCr_2Se_4$, Phys. Rev. Lett. **107**, 186806 (2011).

[2] C. Fang, M. J. Gilbert, X. Dai, and B. A. Bernevig, Multi-Weyl Topological Semimetals Stabilized by Point Group Symmetry, Phys. Rev. Lett. **108**, 266802 (2012).

[3] S.-M. Huang, S.-Y. Xu, I. Belopolski, C.-C. Lee, G. Chang, T.-R. Chang, B. Wang, N. Alidoust, G. Bian, M. Neupane, D. Sanchez, H. Zheng, H.-T. Jeng, A. Bansil, T. Neupert, H. Lin, and M. Z. Hasan, New type of Weyl semimetal with quadratic double Weyl fermions, Proc. Natl. Acad. Sci. **113**, 1180 (2016).

[4] Xiangang Wan, Ari M. Turner, Ashvin Vishwanath, and Sergey Y. Savrasov, Topological semimetal and Fermi-arc surface states in the electronic structure of pyrochlore iridates, Phys. Rev. B **83**, 205101 (2011).

[5] Pavan Hosur, S. A. Parameswaran, and Ashvin Vishwanath, Charge Transport in Weyl Semimetals, Phys. Rev. Lett. **108**, 046602 (2012).

[6] Rudro R. Biswas and Shinsei Ryu, Diffusive transport in Weyl semimetals, Phys. Rev. B **89**, 014205 (2014).

[7] Yuya Ominato and Mikito Koshino, Quantum transport in a three-dimensional Weyl electron system, Phys. Rev. B 89, 054202 (2014).

[8] Björn Sbierski, Gregor Pohl, Emil J. Bergholtz, and Piet W. Brouwer, Quantum Transport of Disordered Weyl Semimetals at the Nodal Point, Phys. Rev. Lett. **113**, 026602 (2014).

[9] Brian Skinner, Coulomb disorder in three-dimensional Dirac systems, Phys. Rev. B **90**, 060202(R) (2014).

[10] Yuya Ominato and Mikito Koshino, Quantum transport in three-dimensional Weyl electron system in the presence of charged impurity scattering, Phys. Rev. B **91**, 035202 (2015).

[11] S. Das Sarma, E. H. Hwang, and Hongki Min, Carrier screening, transport, and relaxation in three-dimensional Dirac semimetals, Phys. Rev. B **91**, 035201 (2015).

[12] Navneeth Ramakrishnan, Mirco Milletari, and Shaffique Adam, Transport and magnetotransport in three-dimensional Weyl semimetals, Phys. Rev. B **92**, 245120 (2015).

[13] Bitan Roy, Robert-Jan Slager, Vladimir Juricic, Global phase diagram of a dirty Weyl semimetal, arXiv:1610.08973 (2016).

[14] Pallab Goswami and Andriy H. Nevidomskyy, Topological Weyl superconductor to diffusive thermal Hall metal crossover in the B phase of UPt_3, Phys. Rev. B **92**, 214504 (2015).

[15] Soumya Bera, Jay D. Sau, and Bitan Roy, Dirty Weyl semimetals: Stability, phase transition, and quantum criticality, Phys. Rev. B **93**, 201302(R) (2016).

[16] Björn Sbierski, Maximilian Trescher, Emil J. Bergholtz, Piet W. Brouwer, Disordered double Weyl node: Comparison of transport and density-of-states calculations, arXiv:1606.06941 (2016).

[17] Qi Chen and Gregory A. Fiete, Thermoelectric transport in double-Weyl semimetals, Phys. Rev. B **93**, 155125 (2016).

[18] Seongjin Ahn, E. H. Hwang, and Hongki Min, Collective modes in multi-Weyl semimetals, Scientific Reports **6**, 34023 (2016).

[19] See Supplemental Material for details of the eigenstates and density of states for multi-Weyl semimetals, density dependence of DC conductivity in multi-Weyl semimetals at zero temperature, temperature dependence of chemical potential and Thomas-Fermi wavevector in multi-Weyl semimetals, and temperature dependence of DC conductivity in multi-Weyl semimetals.

[20] B.Q. Lv, H.M. Weng, B.B. Fu, X.P. Wang, H. Miao, J. Ma, P. Richard, X.C. Huang, L.X. Zhao, G.F. Chen, Z. Fang, X. Dai, T. Qian, and H. Ding, Experimental Discovery of Weyl Semimetal TaAs, Phys. Rev. X **5**, 031013 (2015).

[21] Su-Yang Xu, Ilya Belopolski, Nasser Alidoust, Madhab Neupane, Guang Bian, Chenglong Zhang, Raman Sankar, Guoqing Chang, Zhujun Yuan, Chi-Cheng Lee, Shin-Ming Huang, Hao Zheng, Jie Ma, Daniel S. Sanchez, BaoKai Wang, Arun Bansil, Fangcheng Chou, Pavel P. Shibayev, Hsin Lin, Shuang Jia, M. Zahid Hasan, Discovery of a Weyl fermion semimetal and topological Fermi arcs, Science **349**, 613 (2015).

[22] Neil W. Ashcroft and N. David Mermin, *Solid State Physics*, Brooks Cole (1976).

[23] John Schliemann and Daniel Loss, Anisotropic transport in a two-dimensional electron gas in the presence of spin-orbit coupling, Phys. Rev. B **68**, 165311 (2003).

[24] Karel Výorný, Alexey A. Kovalev, Jairo Sinova, and T. Jungwirth, Semiclassical framework for the calculation of transport anisotropies, Phys. Rev. B **79**, 045427 (2009).

[25] Tsuneya Ando, Alan B. Fowler, and Frank Stern, Electronic properties of two-dimensional systems, Rev. Mod.

Phys. **54**, 437 (1982).

[26] S. Das Sarma, Shaffique Adam, E. H. Hwang, and Enrico Rossi, Electronic transport in two-dimensional graphene, Rev. Mod. Phys. **83**, 407 (2011).

[27] George B. Arfken, Hans J. Weber, and Frank E. Harris, *Mathematical Methods for Physicists* (7th ed.), Academic Press (2012).